Invited Paper

A review of high-efficiency Pancharatnam–Berry metasurfaces

Wang Zhuo, Shulin Sun, Qiong He *, and Lei Zhou *
State Key Laboratory of Surface Physics and Department of Physics,
Fudan University, Shanghai 200438, China
* Email: qionghe@fudan.edu.cn; phzhou@fudan.edu.cn

(Received April 12, 2020)

Abstract: Manipulating circularly polarized (CP) electromagnetic waves as desired is important for a wide range of applications ranging from chiral-molecule manipulations to optical communication, but conventional natural-materials-based devices suffer from bulky configuration and low efficiencies. Recently, Pancharatnam–Berry (PB) metasurfaces have demonstrated strong capabilities to control CP waves in different frequency domains. In this article, we present a concise review on PB metasurfaces for CP light manipulations, focusing mainly on the research works done by our own group. After briefly introducing the working principles of PB metasurfaces, we separately discuss how to construct high-efficiency PB metasurfaces in reflection and transmission geometries, and how to utilize them to control CP waves in different frequency domains, including meta-lensing, meta-hologram, and surface couplers. Finally, we conclude this review with our perspectives on future developments of PB metasurfaces.

Keywords: PB metasurfaces, Geometric phase, Circular polarized light, High-efficiency, Phase gradient

doi:

1. Introduction

The arbitrary control on electromagnetic (EM) wave is always highly desired, not only due to the importance in fundamental sciences, but also for versatile real applications in different areas, such as information communications, national defenses, and energy explorations. However, naturally existing materials exhibit very limited abilities to manipulate light since their EM parameters lie in a very small variation range. Therefore, conventional EM devices, constructed based on the manipulating phase accumulations of propagating waves, usually suffer from the issues of bulky size and low efficiency. Recently, metamaterials (MTMs), artificial materials composed by subwavelength microstructures (also called meta-atoms) arranged in some pre-determined macroscopic orders, were proposed to overcome these bottleneck issues [1]. Many fascinating EM-manipulation effects were achieved based on MTMs in different frequency regimes, such as negative refraction, super imaging, invisibility cloaking, and so on [2-6]. However, constructed by complex 3D metallic structures, MTMs exhibit the shortcomings of inevitable losses and fabrication complexities, especially in high frequency regimes. These issues significantly hinder the further developments and practical applications of MTMs.

Metasurfaces, ultrathin MTMs consisting of planar subwavelength units with tailored EM responses arranged in some specific global orders, offer a more advanced platform to overcome the issues faced by devices made by both natural and MTMs. In contrast to MTMs relying on propagation phases inside the bulk media, metasurfaces fully explore the abrupt phase changes of EM waves at meta-atom interfaces to form certain predetermined phase and/or amplitude distributions on the device surfaces, enabling diversified fascinating wave-manipulation effects with much better performances than those realized with MTMs [7-12], including light bending [13-15], meta-lensing [16-18], propagating wave to surface wave conversion [14, 19, 20], and vector beam generations [7-11, 13, 14, 21-23]. Metasurface-based devices are typically thin, flat, easy to fabricate, and of low losses, all being highly desired in photonic and optic applications. Metasurfaces have become one of the most frontier research fields in photonics. As one important class of metasurfaces, Pancharatnam–Berry (PB) metasurfaces (also called as geometric-phase metasurfaces), whose abrupt phase changes are induced by the orientation of constitutional meta-atoms, have shown great controllability on circularly polarized (CP) EM waves [24-26]. Many fascinating spin-dependent wave-manipulation effects were discovered based on PB metasurfaces, making such systems particularly useful in constructing EM devices for controlling CP waves [26-29].

In this paper, we present a concise review on PB metasurfaces, focusing mainly on the research work done by our own group. We start from introducing the general working principles of PB metasurfaces, and then present our realization and characterization of high-efficiency PB metasurfaces in reflection and transmission geometries, consecutively. We next summarize several representative applications of high-efficiency PB metasurfaces, including meta-holograms, surface-plasmon-polariton (SPP) couplers, and Bessel beam generations. Finally, we conclude this review with our own perspectives on possible future directions of this fast-developing sub-brand of metasurfaces.

2. Working mechanisms of PB metasurfaces

At early stage of metasurface research, metasurfaces were all constructed by planar resonators with different geometrical parameters, and all work for linearly polarized (LP) light. The abrupt phase changes of such resonance-based metasurfaces arise from the resonant frequency shifts of different resonators induced by geometrical parameter tuning. Therefore, such metasurfaces usually suffer from the following issues: narrow working bandwidths, complex design processes and difficulties in fabrications of complex structures with fine differences. PB metasurfaces can largely overcome these challenges, and offer alternative possibilities to control CP waves in additional to LP waves, attracting intensive attention recently.

We first briefly introduce the physical origin of geometric phases adopted in constructing PB

metasurfaces. Consider that an arbitrary anisotropic metallic structure (e.g. a metallic bar) is placed on *xoy* plane and illuminated by a normally incident CP light, the anisotropic nature of the resonator allows the generation of electrical currents flowing along two cross directions exhibiting different amplitudes and phases, generating scattered EM waves with both spin-conserved and spin-reversed components. As early as in 1956, Prof. Pancharatnam already noted that the spin-reversed scattering-wave component can gain an additional phase factor $e^{i2\theta}$, when the planar resonator is rotated by an angle θ with respect to z axis [30]. Such an additional phase, later interpreted as a geometrical phase by Prof. Berry in Ref. [31], exactly equals to half of the solid angle of the area surrounded by two different traces connecting south and north poles on the Poincare Sphere (Fig.1(a)) [32], representing the two spin-reversed scattering processes on two resonators. Thus, the PB phase, dictated solely by the spin-state of input light and the orientation angle of the scatter, exhibits the attractive frequency-dispersionless feature which is totally different from that of the resonance-induced one.

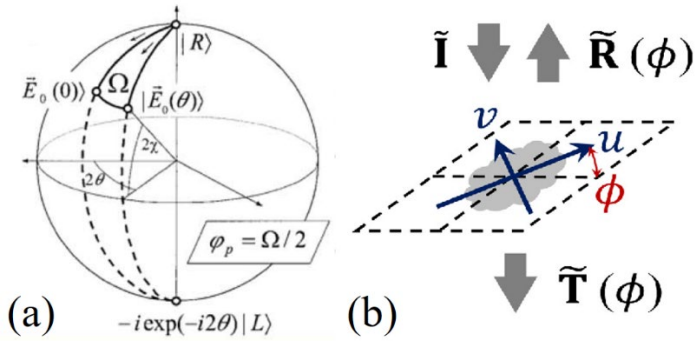

Fig. 1 (a). Illustration of the origin of PB phase based on the Poincare Sphere. (b). Jones Matrix of a metasurface consisting of a 2D array of meta-atoms with local axes rotated with an angle ϕ. (a) reproduced with permission from [32] © 2002,OSA. (b) reproduced with permission from [24] © 2015, Wiley-VCH.

We now discuss quantitatively the working principle of PB metasurfaces by analyzing the EM properties of the constituent meta-atoms with help of the Jones Matrix Method. As shown in Fig.1(b), it is considered that a generic subwavelength meta-atom (periodic repeated to form an infinite plane)is shined by a normally incident light [24]. We choose $\{\hat{u},\hat{v}\}$ to label the two cross axes (e.g., two principle axes of the anisotropic structure) attached to an un-rotated meta-atom. The transmission/reflection properties of the system under study can be well described by two Jones Matrices [24]:

$$\mathbf{T}(0)=\begin{pmatrix} t_{uu} & t_{uv} \\ t_{vu} & t_{vv} \end{pmatrix}, \qquad \mathbf{R}(0)=\begin{pmatrix} r_{uu} & r_{uv} \\ r_{vu} & r_{vv} \end{pmatrix} \tag{1}$$

For the convenience of further analyses, we transform the LP bases $\{\hat{u},\hat{v}\}$ to CP ones with unit vectors $\left\{\hat{e}_+(0)=(\hat{u}+i\hat{v})/\sqrt{2},\ \hat{e}_-(0)=(\hat{u}-i\hat{v})/\sqrt{2}\right\}$, and obtain the corresponding matrices represented by the identity matrix $\hat{I}$ and three Pauli matrices $\{\hat{\sigma}_1,\hat{\sigma}_2,\hat{\sigma}_3\}$ as：

$$T(0) = \frac{1}{2}(t_{uu} + t_{vv})\hat{I} + \frac{i}{2}(t_{uv} - t_{vu})\hat{\sigma}_3 + \frac{1}{2}(t_{uu} - t_{vv})\hat{\sigma}_1 + \frac{1}{2}(t_{uv} + t_{vu})\hat{\sigma}_2 \quad (2)$$

$$R(0) = \frac{1}{2}(r_{uu} + r_{vv})\hat{I} + \frac{i}{2}(r_{uv} - r_{vu})\hat{\sigma}_3 + \frac{1}{2}(r_{uu} - r_{vv})\hat{\sigma}_1 + \frac{1}{2}(r_{uv} + r_{vu})\hat{\sigma}_2 \quad (3)$$

Rotating the meta-atom an angle ϕ with respect to the *z* axis (see Figure 1(b)), we repeat the calculations and find the Jones matrices for the new system as:

$$\begin{aligned} T(\phi) = {} & \frac{1}{2}(t_{uu} + t_{vv})\hat{I} + \frac{i}{2}(t_{uv} - t_{vu})\hat{\sigma}_3 \\ & + \frac{1}{2}(t_{uu} - t_{vv})(e^{-i2\phi}\hat{\sigma}_+ + e^{i2\phi}\hat{\sigma}_-) + \frac{i}{2}(t_{uv} + t_{vu})(-e^{-i2\phi}\hat{\sigma}_+ + e^{i2\phi}\hat{\sigma}_-) \end{aligned} \quad (4)$$

$$\begin{aligned} R(\phi) = {} & \frac{1}{2}(r_{uu} + r_{vv})\hat{I} + \frac{i}{2}(r_{uv} - r_{vu})\hat{\sigma}_3 \\ & + \frac{1}{2}(r_{uu} - r_{vv})(e^{-i2\phi}\hat{\sigma}_+ + e^{i2\phi}\hat{\sigma}_-) + \frac{i}{2}(r_{uv} + r_{vu})(-e^{-i2\phi}\hat{\sigma}_+ + e^{i2\phi}\hat{\sigma}_-) \end{aligned} \quad (5)$$

Here, $\hat{\sigma}_\pm = (\hat{\sigma}_1 \pm i\hat{\sigma}_2)/2$ represents two spin-flip operators satisfying the following relationship $\hat{\sigma}_\pm |\pm\rangle = 0$ and $\hat{\sigma}_\pm |\mp\rangle = |\pm\rangle$, with $|\pm\rangle$ denoting the spin-up (i.e., $\hat{e}_+$) and spin-down (i.e., $\hat{e}_-$) states, respectively. Equations (4) and (5) revealed the underlying physics clearly. Whereas the first two terms in Eqs. (4-5) represents the spin-conserved scatterings without carrying any additional phase, and the last two terms in Eqs. (4-5) represent the spin-reversed scatterings which do carry PB phases $e^{\pm i2\phi}$ depending on the incident spin state. If meta-atoms are arranged with different orientation angles to form PB metasurfaces exhibiting desired phase distributions, one can achieve many fascinating EM wave manipulation effects, such as photonic spin hall effect (PSHE) [24, 25], meta-hologram [33] and meta-lens [28, 29], and so on [34].

3. PB metasurfaces in reflection geometry

Despite of great achievements, most PB meta-devices realized in early years suffer from low-efficiency issue. To solve such an issue, we have theoretically analyzed Eqs. (4-5) and discovered a general criterion to design PB metasurfaces exhibiting 100% efficiency [24]. We consider it as an example of a beam-bending metasurface, formed by arranging identical meta-atoms with successively rotated angles (ϕ, 2ϕ, 3ϕ, 4ϕ...) as shown in Fig. 2(a). Generally, as the PB metasurface is illuminated by a spin-polairzed light, four scattered beams appear, which are the normal/anomalous transmission/reflection modes, as shown in Fig. 2(a). According to Eqs. (4-5) [24, 25], the efficiencies of these four beams are:

$$R_n \equiv \left|(r_{uu} + r_{vv})\right|^2 / 4,\ R_a \equiv \left|(r_{uu} - r_{vv})\right|^2 / 4,\ T_a \equiv \left|(t_{uu} - t_{vv})\right|^2 / 4,\ T_n \equiv \left|(t_{uu} + t_{vv})\right|^2 / 4 \quad (6)$$

where the subscripts “a” and “n” stand for the anomalous and normal modes, respectively.

Obviously, to realize a 100%-efficiency PB meta-device, the multi-mode operation should be avoided, implying that the meta-atom should be totally transparent or reflective. In particle, in pure reflection geometry, where the transmission channel is naturally blocked (i.e. $\tilde{\mathbf{T}}(0) \equiv 0$), the criterion to design a 100%-efficiency PB metasurface is:

$$r_{uu} + r_{vv} = r_{uv} - r_{vu} = 0 \quad (7)$$

implying that the normal-reflection channel should be blocked, thus all incident power is transferred to the anomalous reflection mode with 100% efficiency (see Fig. 2(b)).

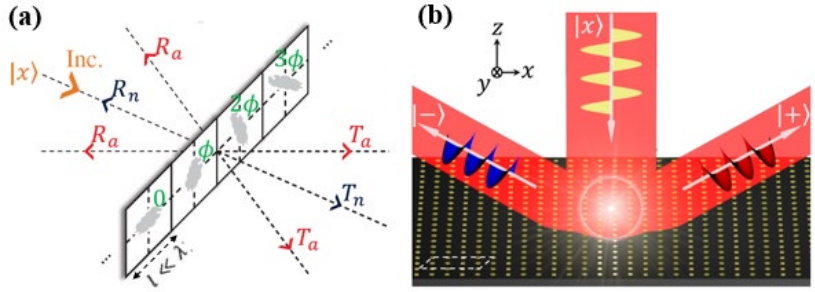

Fig. 2 (a) Anomalous/normal transmissions and reflections (with efficiencies of T_a, R_a, T_n, R_n) generated by a generic PB metasurface consisting of meta-atoms with spatially varying orientation angles $(0, \phi, 2\phi, 3\phi, \cdots)$, under illumination of a LP beam. (b). Schematics of the 100% efficiency PSHE realized at the reflective metasurfaces. (a) reproduced with permission from [25] © 2017, AIP. (b) reproduced with permission from [24]©2015, Wiley-VCH.

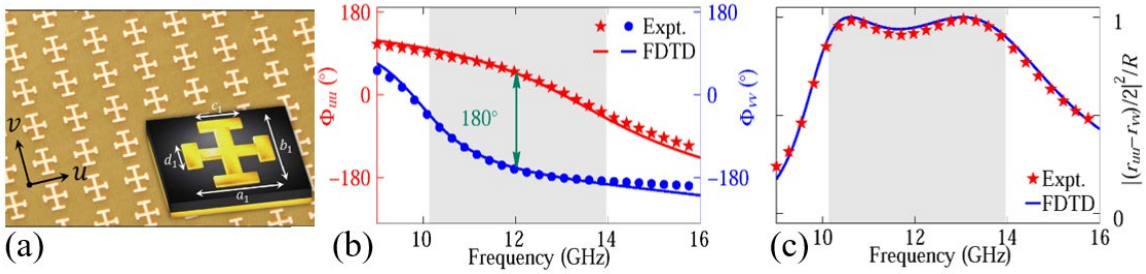

Fig. 3 (a). Sample picture of an array of symmetrical meta-atoms with $a_1 = 4$ mm, $b_1 = 5$ mm, $c_1 = 2.2$ mm, $d_1 = 1.3$ mm (see inset). The thickness and width of metallic wires are 0.05 mm and 0.5 mm, respectively. Spectra of (b) reflection phases (Φ_{uu} and Φ_{vv}) and (c) normalized reflectance $|(r_{uu} - r_{vv})/2|^2 / R$ for the sample shown in (a), obtained by experiments (symbols) and FDTD simulations (line). Here, $R = \left(|r_{uu}|^2 + |r_{vv}|^2 + |r_{uv}|^2 + |r_{vu}|^2\right)/2$ represents the total reflected energy summing up contributions from all four terms in Equation 2, and the gray region in (b) and (c) indicates the working band of our sample which is determined by the condition of $\left[|(r_{uu} + r_{vv})/2|^2 + |(r_{uv} - r_{vu})/2|^2\right]/R < 0.1$. All figures reproduced with permission from [24] © 2015, Wiley-VCH.

Equation (7) provides a general guideline to design 100%-efficiency PB metasurfaces in reflection geometry. We first designed a microwave PB metasurface with meta-atoms exhibiting the mirror symmetry (thus $r_{uv} = r_{vu} \equiv 0$), so that Eq. (7) is reduced to $r_{uu} = -r_{vv}$. Considering the

lossless case, we obtain $|r_{uu}|=|r_{vv}|=1$ thanks to the energy conservation. Thus, the criterion finally reads $\Phi_{vv}-\Phi_{uu}=180^{o}$, implying the meta-atom should function as a perfect reflective half-wave-plate (HWP). Such a meta-atom can be easily designed based on metal-insulator-metal (MIM) configuration [35, 36]. Figure 3(a) illustrates a practical microwave meta-atom design composed by metallic Jerusalem Cross structure and a metallic bottom plate, separated by a dielectric spacer ($\varepsilon=4.3$, thickness d=1.9*mm*). Such a MIM configuration can strongly manipulate the reflection phase to undergo a 180° to -180° variation, as long as frequency passes through the magnetic resonance [36]. Via carefully designing the lateral anisotropy of the meta-atom, one can easily realize any desired phase difference between two orthogonal polarizations. Both experiments and full-wave simulations show that $\Phi_{vv}-\Phi_{uu}$ can keep at about 180^{o} (see Fig. 3(b)) within a quite broad frequency band (10-14*GHz*), leading to nearly 100% efficiency (see Fig. 3(c)). Note that such a broadband property arises from the engineered dispersion cancellations between two low-Q magnetic resonances for two polarizations.

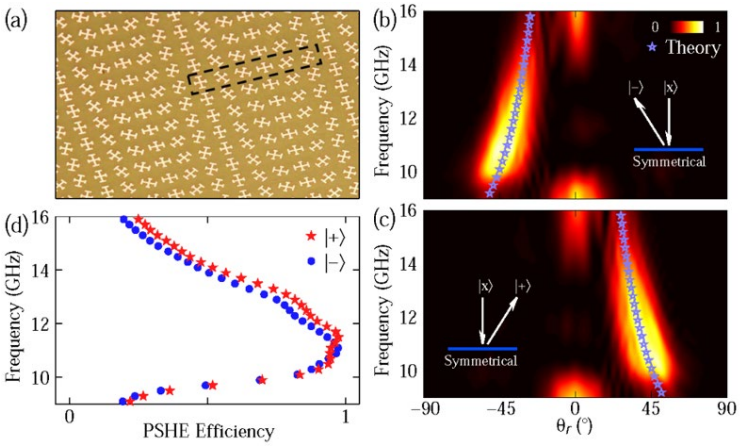

Fig. 4 (a) Pictures of fabricated metasurfaces (sized 504×504 mm^2) formed by symmetrical and l meta-atoms. (b) and (c) Measured normalized scattered-field intensities of LCP and RCP components (color map) versus frequency and detecting angle illuminated by normally incident linearly polarized beams, respectively. (d)PSHE efficiencies versus frequency obtained by analyzing the experimental data in (b, c). Here dotted lines in (b, c) are calculated by Equation 4 under normal-incidence condition. Regions surrounded by black dashed lines in (a) represent the super-cells of PB metasurface. All figures reproduced with permission from [24]© 2015, Wiley-VCH.

With such high-efficiency meta-atom at hand, we successfully fabricated a PB meta-surface and characterized its performances on PSHE. As shown in Fig. 4, shining the meta-surface by normally incident LP waves, far-field measurements clearly illustrated that two CP components are deflected to two distinct directions with in a broad operating band (10-14*GHz*), verifying the desired PSHE (see Figs. 4(b) and 4(c)). Note that the normal reflections are totally suppressed, ensuring the high working efficiency of the meta-device (>90%) (see Fig. 4(d)). Outside of the operating band, the normal reflections increase, degrading the efficiency of PSHE. The deflection angles $\theta_r^{\pm}$ of such anomalously reflected beams is governed by the generalized Snell's law [13-15]:

$$\theta_r^{\pm} = \sin^{-1}(\sin\theta_i + \xi^{\pm} / k_0) \qquad (8)$$

With θ_i and $k_0 = \omega / c$ being the incident angle and the wave-vector in vacuum, respectively. Equation (8) indicates that the deflection angle is determined by the phase gradient $\xi^{\pm} = \pm 2\phi / l$, which is experimentally verified based on our PB metasurfaces (dotted lines in Figs. 4(b) and 4(c)).

4. PB metasurfaces in Transmission geometry

Although reflective PB metasurfaces can readily achieve high working efficiencies, 100% efficiency PB metasurfaces in transmission geometry are even more desired in applications. Unfortunately, they are also more difficult to realize, since more channels exist for scattered waves to travel in such a configuration. In fact, some early works even theoretically and experimentally demonstrated that the working efficiency of an ultrathin PB metasurfaces was bounded by 25% [37, 38]. We analyzed this question in details and found through Eq. (6) that 100% efficiency transmissive PB metasurfaces can be achieved, as long as the following criterions

$$r_{uu} = r_{vv} = 0, \quad |t_{uu}| = |t_{vv}| = 1, \quad \arg(t_{uu}) = \arg(t_{vv}) \pm \pi \qquad (9)$$

are satisfied. Equation (9) requires that the meta-atom should not only be totally transparent, but should also function as a HWP in transmission mode [24]. However, we found that a single-layer meta-atom with purely electric response can never satisfy the above requirements, since an electrical dipole always radiates symmetrically to both sides, not allowing for independent tuning on the reflected and transmitted waves.

In 2017, based on effective-current analyses, we found that the desired meta-atom should contain both electric and magnetic responses, resulting in destructive interference at reflection side and constructive interference at transmissive side (see Fig. 5(a)) [25]. Inspired by our previous work [19, 39, 40], we designed such transmissive meta-atom based on the ABA tri-layer configuration in the microwave regime, and experimentally characterized its transmission properties. As shown in Fig. 5(b), the meta-atom consists of three metallic layers, with layer A being a metallic bar and layer B a holey metallic film loaded with a metallic bar. Two adjacent metallic layers are separated by a FR4 dielectric film. Both experiments and simulations demonstrated that the designed meta-atom is optically transparent for both polarizations with the transmission phase difference of about 180° inside a frequency window centered at 10.6 *GHz*. Prefect transparencies of such meta-atom for two polarizations are governed two different mechanisms, so that the associated transmission phase are naturally different [25]. We next employed the designed meta-atom as a basic element to construct a transmissive PB metasurface with inter-particle rotation angle of 30° (see Fig. 6a), and experimentally characterize its PSHE performances. Figures 6(b)-6(f) depict the measured spin-dependent scattering patterns of our sample at both transmission and reflection sides, showing that only the anomalous transmission survives with all other three modes suppressed, within the

frequency band of 10.1-10.9 *GHz*. Outside this operating band, anomalous transmission decreases significantly. Experimentally measured PSHE efficiency reaches 91% at 10.5*GHz*, which is in good agreement with full-wave simulation results (94%). Note that the total thickness of our metasurfaces is only 4 *mm*, which is approximately λ/8, it is worthy noting that our arguments on achieving the 100% efficiency transmissive metasurfaces are in the same spirit as previous discussions, such as Huygens' metasurfaces [41, 42] or dielectric metasurfaces [23, 34, 43].

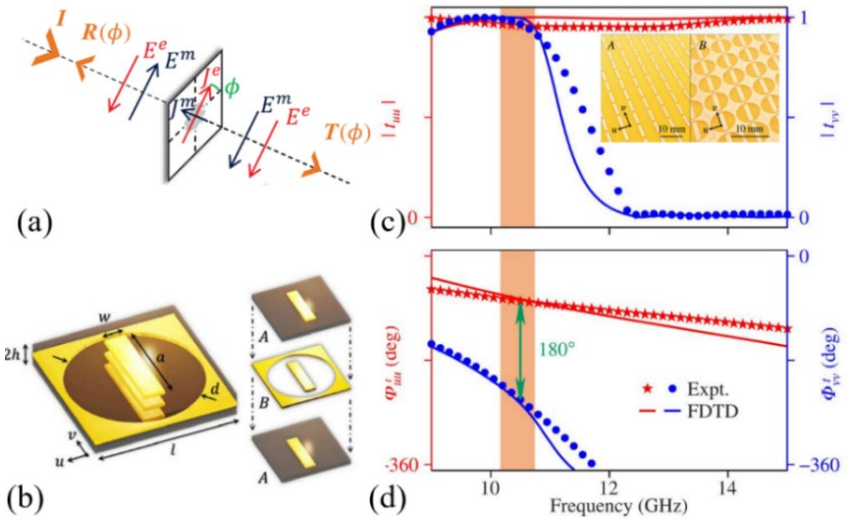

Fig. 5 (a) Schematics of a ϕ-orientated meta-atom with transmission/reflection characteristics described by two Jones' matrices $\boldsymbol{T}$ and $\boldsymbol{R}$, and the E fields radiated from the electric and magnetic currents ($\vec{J}_e$ and $\vec{J}_m$) generated on the meta-atom. (b). Schematics of the ABA meta-atoms and layer A and layer B. (c)(d)measured and full-wave simulated spectra of transmission amplitude and phase for the metasurface composed by periodic array of the ABA meta-atoms. Inset: picture of fabricated layer A and layer B. all figurs reproduced with permission from [24] © 2017, AIP.

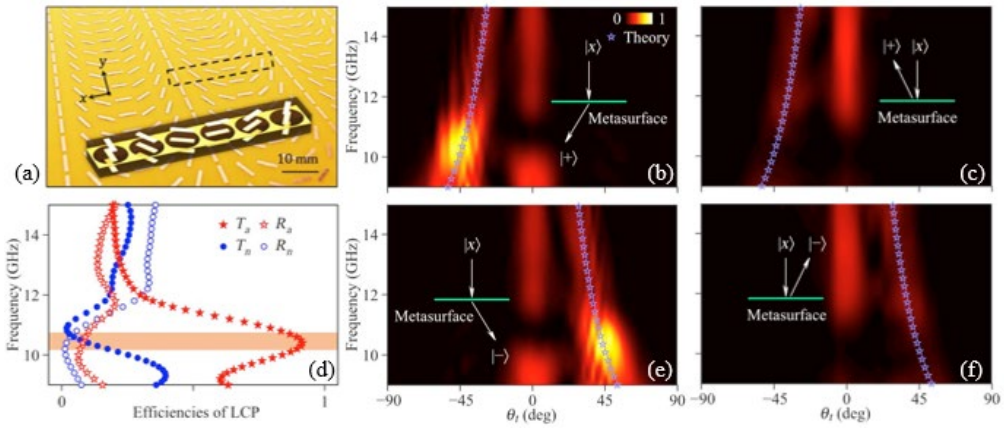

Fig. 6 (a) Picture of fabricated PB metasurefaces formed by ABA meta-atoms. Measured scattered-field intensities in the (b),(c) transmission and (e)(f) reflection sides as function of frequency and the detecting angle for the PB metasurface illuminated by normally incident LP wave. (d) Absolute efficiencies of the four modes versus frequency for the PB metasurface obtained through analyzing experimental data in (b),(c),(e),(f). Blue starts represent the results calculated based on the generalized Snell's law. All figures reproduced with permission from [24] © 2017, AIP.

5. Applications of high-efficiency PB metasurfaces

PB metasurfaces have significantly expanded our controllability on spin-polarized light, stimulating many fascinating applications [21]. In what follows, we will introduce some of representative applications of PB metasurfaces.

In 2015, we demonstrated that reflective PB metasurfaces could work as efficient and broadband polarization detectors [24]. As shown in Fig.7(a), our PB metasurfaces can efficiently reflect two spin components of input wave with unknown polarization to two different directions. Measuring the amplitudes and phases of these two anomalous reflection modes simultaneously, we can retrieve the original polarization state of the impinging wave. As a comparison, we directly characterize the orientation angle χ and ellipticity angle ψ of the input wave (see inset to Figure 6(a)). Excellent agreement is noted between the retrieved and directly measured results (see Fig. 6(b)). Compared to conventional polarization detectors, high-efficiency operation and robustness are the key advantages of our approach. In a parallel line, other groups also reported such efficient approach for polarization detection in different frequency regime [44-46]. As shown in Figs. 6(c) and 6(d), Pors *et al.* demonstrated simultaneous determination of Stokes' parameters of input light based on a plamonic PB metasurfaces in reflection geometry at the working wavelength of 800 *nm* [45].

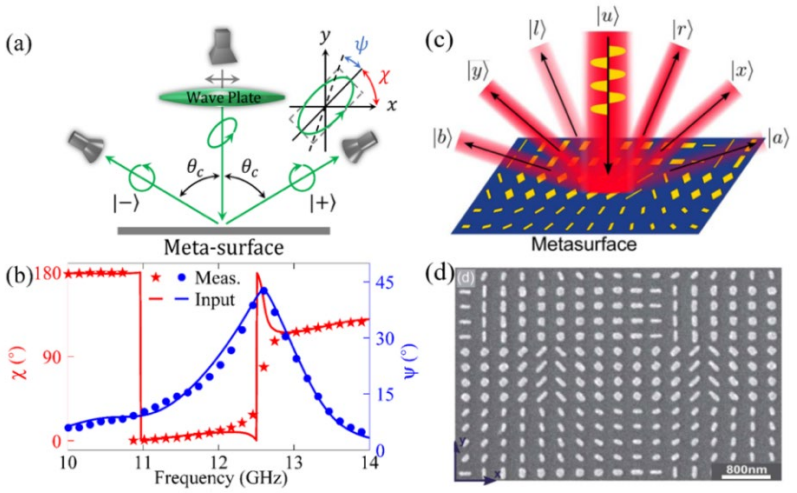

Fig. 7 (a) Schematics of our polarization-detecting experiments. The inset depicts a general elliptic polarization state defined by the orientation angle χ and the degree of ellipticity ψ. (b) Polarization states of the input beam are measured by our experiments (symbols), and are compared with the input values (lines). (c) Illustration of the metagrating's working principle. An incoming beam with an unknown polarization state is on reflection represented in the bases $(\hat{x},\hat{y})$, $(\hat{a},\hat{b})$, and $(\hat{r},\hat{l})$, thereby allowing one to determine the Stokes parameters and, hence, the state of polarization without the need of multiple measurements or an interferometric setup. (a) and (b) reproduced with permission from [24] © 2015, Wiley-VCH. (c) and (d) reproduced with permission from [45] © 2015,OSA.

PB metasurfaces were also proposed to work as direction-controllable SPP couplers, as long as the designed phase gradient on such metasurfaces exceeds free-space wave-vectors [47-49]. Such an idea originates from the pioneering work of Ref. [14], where gradient metasurfaces were first demonstrated as SPP couplers for LP waves. However, early demonstrations on PB meta-couplers suffered from severe low-efficiency issue (<10%), due to both direct reflection at the coupler surface and the mode mismatch between the coupler and the guiding-out plasmonic structure. Specifically, in previous designs, the constituent meta-atoms did not satisfy our criterion to achieve 100% working efficiency generating large specular reflections, and the guiding-out plasmonic metals usually only supported SPP modes with transvers-magnetic (TM) polarization while the incident CP light contained both transvers-electric (TE) and TM components. We recently proposed a new scheme to overcome these issues [20]. The improved performances were obtained based on the following two crucial steps. First, we designed a 100%-efficiency PB meta-atom based our criterion and then employed it as the building block to construct our PB meta-coupler, which naturally ensured nearly zero specular reflections at the device surface. Second, we carefully designed an artificial "plasmonic metal" supporting both TM and TE polarized spoof SPP in the microwave regime (see Fig. 8(c)), which was then used as the guiding-out structures. Based on the device with these improvements, we performed near-field (see Fig.8 (b-d)) and far-field measurements to demonstrate that both TE and TM polarized surface waves generated on the meta-coupler could be efficiently guided out to flow as eigen SPPs on the "plasmonic metal", and the final conversion efficiency from incident propagating wave to SPPs reach as high as 78% and could be further improved.

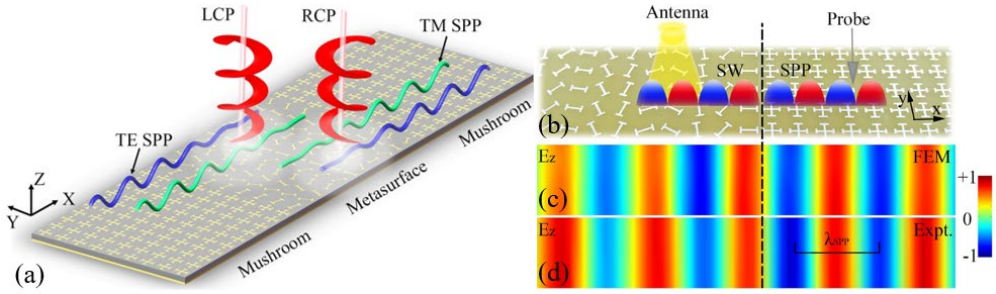

Fig. 8 (a) Schematics of the realistically designed PB meta-coupler illuminated by the LCP or CP waves, producing high-efficiency chirality-controlled SPPs. (b) Sample picture and experimental setup to demonstrate the SPP excitation performance of the proposed PB meta-coupler. (c)(d) near-field measured and FEM simulated Ez field distributions (real part) above PB meta-coupler at 10 *GHz*, respectively. All figures are reproduced from [20].

PB metasurfaces were also excellent platforms to realize meta-holograms, with required phase distributions easily realized by setting appropriate orientation angles of all constitutional meta-atoms [50-54]. However, early reported PB meta-holograms exhibit low working efficiencies [50-52], again due to the fact that those meta-atoms were not designed based on the 100%-efficiency criterion. In Ref. [53], Zhang *et al.* independently discovered the criterion to realize 100% efficiency PB meta-atoms in reflection geometry, and experimentally demonstrated a meta-

hologram with working efficiency of ~80% at optical frequencies. The adopted meta-atom is also a MIM nano-structure with top resonator as a metallic bar, functioning as an HWP with polarization conversion efficiency over 80% within a wavelength bandwidth covering 550-1000*nm*. In addition, the spin-sensitive responses of PB metasurfaces motivated many researchers to realize chirality-multiplexed mete-devices in different wavelength ranges [27]. Wen *et al.* experimentally demonstrated helicity-multiplexed holography with high-efficiency PB metasurfaces, composed of two sets of MIM meta-atoms with independently controlled orientations to encode two different holographic images (i.e. a bee and a flower for RCP and LCP light). The measured working efficiency of such a device reaches 40% at 900*nm* [27]. However, the high-efficiency meta-holograms in reflection geometry is sometimes inconvenient for real applications. Recently, many researchers have turned to study dielectric meta-atoms, which are good candidates to realize high-efficiency transmissive PB metasurfaces in the optical regime, where plasmonic metals all suffer from the loss issue. In 2016, Capasso's group realized a high efficiency PB meta-hologram at visible wavelengths, utilizing high-aspect-ratio TiO_2 nano-fins with anisotropic cross sections as building blocks. The measured maximum working efficiency of such a meta-device reaches 81%, which is quite impressive [18, 55]. Recently, many fascinating meta-holograms were reported based on PB metasurfaces in different frequency regimes made by different materials [54, 56], and we could not list all of them due the limited space.

PB metasurfaces were also widely used to generate spin-polarized special beams. One typical example is the CP Bessel beam (BB), which exhibits non-diffraction and self-healing properties, being highly desired for applications such as chiral molecular manipulations. In 2018, we employed a high-efficiency transmissive meta-HWP (see Fig. 5) as the building block to design a transmissive meta-axicon exhibiting the following phase distribution $\phi(x,y) = k_{//}\sqrt{x^2+y^2}$ for incident CP

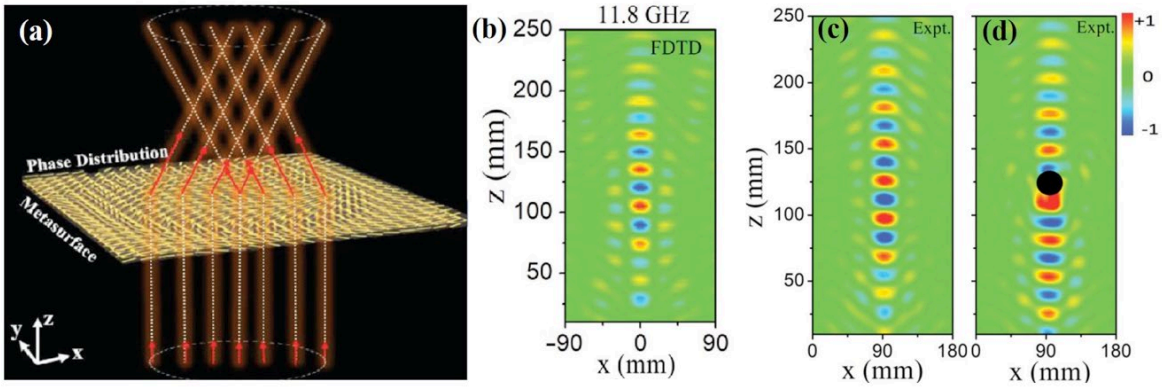

Fig. 9(a). Schematic of meta-axicon based on a 100%-efficiency PB meta-atom in ABA configuration for Bessel beam generation with high efficiencies. (b),(c) FDTD simulated and measured Ey field distributions on the xz-plane at the transmission side of the designed BB generator at 11.8*GHz*, respectively (d) Experimental verification of self-healing effect of the generated BB based on Ey distribution of the meta-axicon with presence of a metallic sphere (diameter D=15*mm*). all figures reproduced with permission from [28] © 2018, AIP.

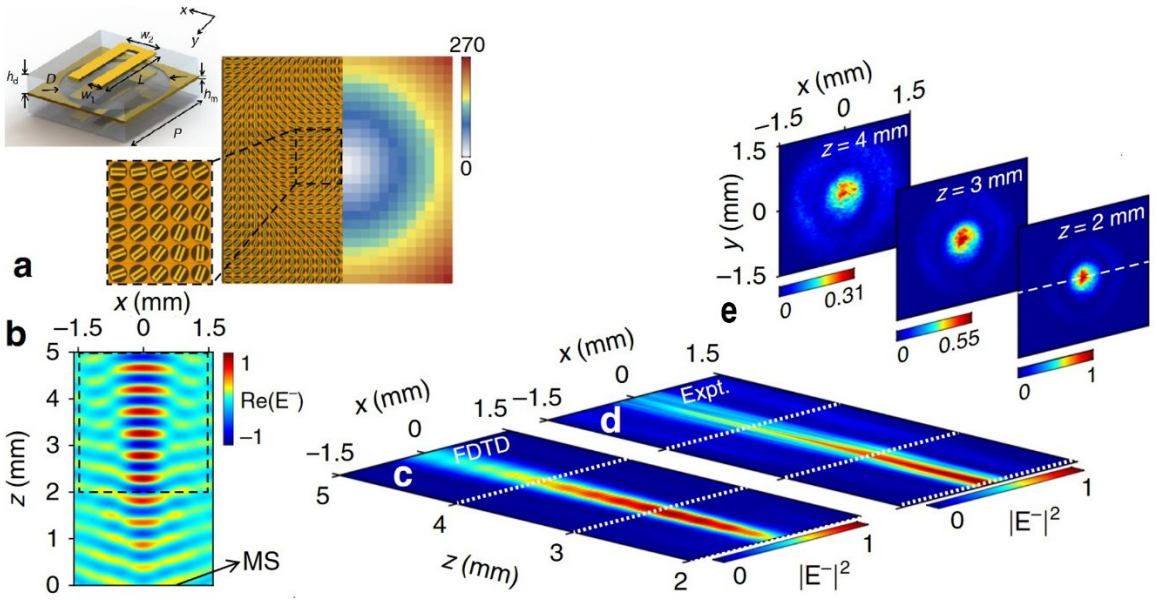

Fig. 11 (a) Schematic of meta-atom design and picture of part of a fabricated CP Bessel beam generator which is a PB metasurface (left panel) designed based on a particular transmission-phase distribution (right panel). (b) FDTD simulated $\mathrm{Re}(E^{-})$ distribution on the xz plane with y = 0 *mm* for our metasurface (placed at z = 0 *mm*) shined by a normally incident x-polarized THz beam at 0.66*THz*. (c) FDTD simulated and (d) z-scan measured $|E^{-}|^2$ distributions inside the area surrounded by black dashed lines in (b), under exactly the same conditions as in (b). (e) Measured $|E^{-}|^2$ distributions on x-y planes with z=2, 3 and 4 *mm*, respectively. all figures reproduced from [29].

microwave (see Fig. 9(a)) [28]. Both full-wave simulations and microwave experiments demonstrated the non-diffraction and self-healing properties of the BBs generated by such a device under the excitation of a CP microwave (see Figs. 9(b-d)). The measured (simulated) working efficiency of our meta-devices reaches 91% (~92%) at 12*GHz*, and the self-healing effect is insensitive to the shape and position of the metallic scatter. We have further extended our meta-axicon design to the terahertz (THz) regime, where the generated CP BBs could find more important applications, such as biological sensing and telecommunications [29]. The adopted plasmonic meta-atom is still a multilayer structure in ABA configurations. As shown in Fig. 10(a), layer A in our meta-atom is a U-shaped metallic resonator, layer B is a metallic plate with holes loaded with the same U-shaped resonator, and two polyimide spacers are employed to separate the three metallic layers. In this design, interlayer couplings can introduce appropriate effective magnetic currents, which help making the whole structure transparent. Meanwhile, the U-shape can provide more freedoms to generate lateral anisotropy for EM responses of different polarizations. Fig. 10(b) depicts the FDTD simulated $\mathrm{Re}(E^{-})$ (i.e. RCP field component) distribution on *x–y* plane at the transmission side of our PB device, under the illumination of an *x*-polarized normally incident beam at 0.66*THz*. Clearly, an RCP BB is generated with non-diffracting properties. We then have fabricated out the sample and experimentally characterized

the properties of CP BBs generated, with a THz digital holographic imaging system [57, 58]. Both simulated and measured intensity profiles well illustrate the non-diffracting features of the generated BB at $0.66THz$. In addition, Fig. 10(e) depicts the measured intensity distributions of the BB on *xy* planes at different longitudinal position, showing very well-behaved patterns with rotation symmetries. Thanks to the high efficiency of the constitutive PB meta-atom, such a generated CP BB is very clean, which does not suffer from the interferences from the normal transmission mode.

Before closing this subsection, we note that PB metasurfaces offer researchers great capabilities to construct spin-dependent meta-devices with diversified functionalities. However, due to the limitation of the paper length, we are not able to mention other important applications such as meta-lens [59–61], vortex beam generation [25, 62–64] and helicity-multiplexed meta-devices [48, 51, 65-70].

5. Conclusions and perspectives

To summarize, we present a short review on PB metasurfaces, focusing mainly on the work done in our own group. After briefly introducing the working principles of PB metasurfaces, we present the general criterions that we have discovered to design 100%-efficiency PB metasurfaces in both reflection and transmission geometries, which are the crucial steps to overcome the low-efficiency issues persisting in many PB metasurfaces realized in early years. We next introduce our efforts on constructing PB metasurfaces based on the discovered criterions and characterizing their controllability on spin-polarized EM waves. We finally summarize several important applications of such high-efficiency PB metasurfaces in different frequency regimes, including polarization detection, meta-hologram, SPP-couplers, and special-beam generations. Although we mainly focus on those works done in our own group, we hope that this short review can help the readers to deepen their understanding on PB metasurfaces, and provide them useful guidance for designing their own PB meta-devices in the future.

Before concluding this review, we would like to mention a couple of promising research directions on PB metasurfaces, based on our perspectives.

A. **Meta-devices based on PB and resonant mechanisms.** Although PB metasurfaces can manipulate CP EM waves with different chirality, the achieved functionalities for LCP and RCP light are usually locked. To realize meta-devices exhibiting independent functionalities on controlling CP waves with different handedness, one needs to exploit both the PB mechanism and the resonance one, which is now a very hot topic in metasurface research.
B. **Active and tunable PB metasurfaces/meta-devices.** While many fascinating wave-manipulation effects have been demonstrated with PB metasurfaces/meta-devices, the achieved

functionalties are fixed once the devices are fabricated out. It is thus highly desired to make tunable PB meta-devices exhibiting actively tunable manipulations on CP waves with fast switching speed, which is now another hot topic in the metasurface research.

Acknowledgments

This work was funded by the National Natural Science Foundation of China (No. 11734007, No. 91850101, No. 11674068, and No. 11874118), the National Key Research and Development Program of China (No. 2017YFA0303504 and No. 2017YFA0700201), the Natural Science Foundation of Shanghai (No. 18ZR1403400).

References

[1] N. Engheta, and R. W. Ziolkowski. *Metamaterials: Physics and Engineering Explorations*, John Wiley & Sons, Inc., Hoboken, NJ, USA(2006).

[2] Y. Liu, and X. Zhang. *Chem. Soc. Rev. 40*, 2494(2011).

[3] D. Schurig, J. J. Mock, B. J. Justice, et al. *Science 314*, 977(2006).

[4] U. Leonhardt. *Science*, *312*, 1777(2006)

[5] J. B. Pendry, D. Schurig, and D. R. Smith. *Science 312*, 1780 (2006)

[6] Y. Lai, J. Ng, H. Chen, et al. *Phys. Rev. Lett. 102*, 253902(2009)

[7] N. Yu, and F. Capasso. *Nat. Mater. 13*, 139(2014).

[8] S. B. Glybovski, S. A. Tretyakov, P. A. Belov, et al. *Phys. Rep. 634*, 1(2016).

[9] F. Ding, A. Pors, and S. I. Bozhevolnyi. *Reports Prog. Phys. 81*, 026401(2017).

[10] H.-T. Chen, A. J. Taylor, and N. Yu. *Reports Prog. Phys. 79*, 076401(2016).

[11] Q. He, S. Sun, S. Xiao, et al. *Adv. Opt. Mater. 6*, 1800415(2018).

[12] S. Sun, Q. He, J. Hao, et al. *Adv. Opt. Photonics 11*, 380(2019).

[13] N. Yu, P. Genevet, M. a. Kats, et al. *Science. 334*, 333(2011).

[14] S. Sun, Q. He, S. Xiao, et al. *Nat. Mater. 11*, 426(2012).

[15] S. Sun, K.-Y. Yang, C.-M. Wang, et al. *Nano Lett. 12*, 6223(2012).

[16] F. Aieta, P. Genevet, M. a Kats, et al. *Nano Lett. 12*, 4932(2012).

[17] X. Li, S. Xiao, B. Cai, et al. *Opt. Lett. 37*, 4940(2012).

[18] M. Khorasaninejad, W. T. Chen, R. C. Devlin, et al. *Science 352*, 1190(2016).

[19] W. Sun, Q. He, S. Sun, et al. *Light Sci. Appl. 5*, e16003(2016).

[20] J. Duan, H. Guo, S. Dong, et al. *Sci. Rep. 7*, 1354(2017).

[21] H.-H. Hsiao, C. H. Chu, and D. P. Tsai. *Small Methods. 1*, 1600064(2017).

[22] S. Kruk, and Y. Kivshar. *ACS Photonics. 4*, 2638(2017).

[23] M. Decker, and I. Staude. *J. Opt. 18*, 103001(2016).

[24] W. Luo, S. Xiao, Q. He, et al. *Adv. Opt. Mater. 3*, 1102(2015).

[25] W. Luo, S. Sun, H.-X. Xu, et al. *Phys. Rev. Appl. 7*, 044033(2017).

[26] G. Zheng, H. Mühlenbernd, M. Kenney, et al. *Nat. Nanotechnol. 10*, 308(2015).

[27] D. Wen, F. Yue, G. Li, et al. *Nat. Commun. 6*, 8241(2015).

[28] Z. Wang, S. Dong, W. Luo, et al. *Appl. Phys. Lett. 112*, 191901(2018).

[29] M. Jia, Z. Wang, H. Li, et al. *Light Sci. Appl. 8*, 16(2019).

[30] S. Pancharatnam. *Proc. Indian Acad. Sci. - Sect. A. 44*, 398(1956).

[31] M. V. Berry. *Proc. R. Soc. A Math. Phys. Eng. Sci. 392*, 45(1984).

[32] Z. Bomzon, G. Biener, V. Kleiner, et al. *Opt. Lett. 27*, 1141(2002).

[33] G. Zheng, H. Mühlenbernd, M. Kenney, et al. *Nat. Nanotechnol. 10*, 308(2015).

[34] A. Arbabi, Y. Horie, M. Bagheri, et al. *Nat. Nanotechnol. 10*, 937(2015).

[35] J. Hao, Q. Ren, Z. An, et al. *Phys. Rev. A. 80*, 23807(2009).

[36] J. Hao, Y. Yuan, L. Ran, et al. *Phys. Rev. Lett. 99*, 63908(2007).

[37] A. Arbabi, and A. Faraon. *Sci. Rep. 7*, 43722(2017).

[38] X. Ding, F. Monticone, K. Zhang, et al. *Adv. Mater. 27*, 1195(2015).

[39] W. Sun, Q. He, J. Hao, et al. *Opt. Lett. 36*, 927(2011).

[40] L. Zhou, W. Wen, C. T. Chan, et al. *Phys. Rev. Lett. 94*, 243905(2005).

[41] C. Pfeiffer, and A. Grbic. *Phys. Rev. Appl. 2*, 044012(2014).

[42] C. Pfeiffer, and A. Grbic. *197401*, 1(2013).

[43] D. Lin, P. Fan, E. Hasman, et al. *Science. 345*, 298(2014).

[44] A. Shaltout, J. Liu, A. Kildishev, et al. *Optica. 2*, 860(2015).

[45] A. Pors, M. G. Nielsen, and S. I. Bozhevolnyi. *Optica. 2*, 716(2015).

[46] P. C. Wu, J.-W. Chen, C.-W. Yin, et al. *ACS Photonics. 5*, 2568(2018).

[47] J. Lin, J. P. B. Mueller, Q. Wang, et al. *Science. 340*, 331(2013).

[48] S. Xiao, F. Zhong, H. Liu, et al. *Nat. Commun. 6*, 8360(2015).

[49] S.-Y. Lee, K. Kim, S.-J. Kim, et al. *Optica. 2*, 6(2015).

[50] Y. W. Huang, W. T. Chen, W. Y. Tsai, et al. *Nano Lett. 15*, 3122(2015).

[51] L. Huang, H. Mühlenbernd, X. Li, et al. *Adv. Mater. 27*, 6444(2015).

[52] X. Li, L. Chen, Y. Li, et al. *Sci. Adv. 2*, e1601102(2016).

[53] G. Zheng, H. Mühlenbernd, M. Kenney, et al. *Nat. Nanotechnol. 10*, 308(2015).

[54] K. Huang, Z. Dong, S. Mei, et al. *Laser Photon. Rev. 10*, 500(2016).

[55] R. C. Devlin, M. Khorasaninejad, W. T. Chen, et al. *Proc. Natl. Acad. Sci. 113*, 10473(2016).

[56] M. Khorasaninejad, A. Ambrosio, P. Kanhaiya, et al. *Sci. Adv. 2*, e1501258(2016).

[57] Z. Wu, X. Wang, W. Sun, et al. *Opt. Express. 26*, 1506(2018).

[58] Z. Wu, X. Wang, W. Sun, et al. *Sci. Rep. 7*, 13929(2017).

[59] S. Wang, P. C. Wu, V.-C. Su, et al. *Nat. Commun. 8*, 187(2017).

[60] S. Person, M. Jain, Z. Lapin, et al. *Nano Lett. 13*, 1806(2013).

[61] W. T. Chen, A. Y. Zhu, V. Sanjeev, et al. *Nat. Nanotechnol. 13*, 220(2018).

[62] L. Huang, X. Chen, H. Mühlenbernd, et al. *Nano Lett. 12*, 5750(2012).

[63] E. Karimi, S. A. Schulz, I. De Leon, et al. *Light Sci. Appl. 3*, e167(2014).

[64] X. Ma, M. Pu, X. Li, et al., *Sci. Rep. 5*, 10365(2015).

[65] J. P. Balthasar Mueller, N. A. Rubin, R. C. Devlin, et al. *Phys. Rev. Lett. 118*, 113901(2017).

[66] S. Choudhury, U. Guler, A. Shaltout, et al. *Adv. Opt. Mater. 5*, 1700196(2017).

[67] D. Wen, S. Chen, F. Yue, et al. *Adv. Opt. Mater. 4*, 321(2016).

[68] S. Wang, X. Wang, Q. Kan, et al. *Opt. Express 23*, 26434(2015).

[69] E. Maguid, I. Yulevich, M. Yannai, et al. *Light Sci. Appl. 6*, e17027(2017).

[70] E. Maguid, I. Yulevich, D. Veksler, et al. *Science 352*, 1202(2016).